CERN-PPE/91-08
18 January 1991

EUROPEAN ORGANIZATION FOR NUCLEAR RESEARCH

X-rays from Antiprotonic ^{3}He and ^{4}He

M. Schneider, R. Bacher, P. Blüm, D. Gotta, K. Heitlinger,
W. Kunold, D. Rohmann

Institut für Kernphysik und Institut für Experimentelle
Kernphysik der Universität, Kernforschungszentrum Karlsruhe
GmbH,
Postfach 3640, D–7500 Karlsruhe 1, Germany

J. Egger, L.M. Simons

Paul Scherrer Institut, CH–5432 Villigen (PSI), Switzerland

K. Elsener

CERN, CH–1211 Geneva 23, Switzerland

Abstract

Antiprotonic X–rays from the helium isotopes have been observed at pressures of 36, 72, 375 and 600 mbar. The antiproton beam from LEAR with momenta of 309 and 202 MeV/c has been stopped at these pressures using the cyclotron trap. The X–rays were detected with Si(Li) and intrinsic Ge semi–conductor detectors. Absolute X–ray yields were determined and the strong interaction 2p shifts and the 2p and 3d broadenings measured to be ε_{2p} = –(17±4) eV, Γ_{2p} = (25±9) eV, and Γ_{3d} = (2.14±0.18) meV for $\bar{p}^3He$ and ε_{2p} = –(18±2) eV, Γ_{2p} = (45±5) eV and Γ_{3d} = (2.36±0.10) meV for $\bar{p}^4He$.

(accepted for publication in Z. Phys. A – Atomic Nuclei)

1. Introduction

The helium isotopes can be regarded as the most interesting (but by far not simple systems) where the description of the $\bar{p}$–nucleus interaction in terms of the elementary antiproton–nucleon interaction can be tested [1–3].

The aim of this experiment was to determine broadenings and shifts due to strong interaction of the last observable X–ray transitions, as well as the study of the pressure dependence of the atomic cascade. (Pre–LEAR) experiments suffered from the very poor antiproton fluxes requiring the use of fairly large liquid or high pressure helium targets [4–6]. The operation of LEAR allows for the accumulation of high statistics and a substantial reduction of the target density. At pressures below 1000 mbar the influence of the Stark mixing decreases rapidly thus yielding an increase of the X–ray intensities, a high sensitivity to the cascade parameters, and an improved measurement of both weak transitions and transitions with small hadronic shifts and widths, where good statistics are required.

2. Experiment

The measurement was performed in 3 periods in the LEAR M1–area with beam momenta of 309 (measurement I) and 202 MeV/c (measurement II and III). Using the cyclotron trap, the experiment could be performed at very low gas pressures [7]. The basic principle of this apparatus is to wind up the range curve of a particle beam in a weak focussing magnetic field. After entering the target chamber, placed in the gap of the split–coil magnet, the antiprotons pass a degrader–scintillator arrangement, which matches the beam momentum to the momentum accepted by the cyclotron trap ($\sim$ 90 MeV/c). The particles then loose energy in the target gas itself and spiral to the center of the trap. The stop efficiency f_{stop} (ratio of antiprotons stopped at the center in the target gas to the number of incoming antiprotons N_{in}) is shown in Fig. 1. The X–rays were measured with various Si(Li) (Si I, II and III) and planar intrinsic Ge detectors (Ge I and II) mounted in the bore holes of the magnet. The set–up parameters for this experiment are given in table 1. Further details of the set–up are described elsewhere [8–10]. The determination of absolute yields requires knowledge of the stop efficiency f_{stop}, the in–beam efficiency ϵ_{det}, and the effective solid angle ($\Delta\Omega/4\pi$) of the detectors.

In measurement I, f_{stop} was determined indirectly via the intensity I_{4-3} of the $\bar{p}^4$He(4–3) transition, which is not affected by the strong interaction:

$$f_{stop} = I_{4-3} / (N_{in} \cdot Y_{4-3} \cdot \epsilon_{det} \cdot \left[\frac{\Delta\Omega}{4\pi}\right]).$$

As absolute yields could not be determined in measurement I, the prediction from a cascade calculation [11] was used for the yield Y_{4-3} of the $\bar{p}^4$He(4–3) transition. The accuracy of this prediction is better than 10% for the transitions not affected by the strong interaction (implied by comparison of calculations for myonic helium [12]). Efficiency, energy and energy resolution calibrations were performed in beam with calibrated ^{54}Mn and ^{241}Am sources between 5.4 and 59.5 keV. The efficiency calibration was extended to energies below 5 keV with X–ray fluorescence sources. The size of the stop volume was determined using various collimators in the bore holes of the magnet (thus allowing for the calculation of the solid angle). The intensities were corrected for absorption in the 12 μm Be window of the target chamber and the 2 mm air gap between the windows of the target chamber and the detector.

For measurement II, f_{stop} was determined directly from the time–of–flight between the scintillator detecting the incoming antiprotons and a set of plastic scintillators (attached to the target chamber), which detected charged annihilation products. This method, described in detail elsewhere [10], permitted identification of the X–rays originating from the stops in the gas volume and determination of absolute yields. The in–beam response function of the detectors was monitored with calibrated ^{57}Co and ^{241}Am sources. In addition, a ^{73}As and a ^{75}Se source were used in the measurement of $\bar{p}^3$He and $\bar{p}^4$He, respectively. The energies of the X–rays emitted by the daughter atoms are just below (Kα) and above (Kβ) the $\bar{p}$ He (3–2) transition energies.

In measurement III, the method of complete ionization of antiprotonic atoms at low pressures (e.g. antiprotonic nitrogen at equivalent pressure) was used [9], allowing for an in–beam calibration of energy, relative efficiency and resolution with identical conditions. The numerous lines of saturated X–ray transitions, not affected by strong interaction, yield directly the response functions of the detectors after a correction to self absorption. The relation to absolute efficiencies is obtained from a calibrated ^{57}Co source. Due to the narrower stop distribution in measurement II and III, the solid angle is given by the active areas and the positions of the detectors. The size of the stop

volume is known to be less than 100 cm^3 from simulations of the antiproton trajectories [7].

In fig. 2a the X–ray spectrum of $\bar{p}^4$He at 600 mbar is shown (measurement I). The absence of antiprotonic X–rays originating from the materials of the wall of the target chamber confirms the small size of the stop volume. In fig. 2b the X–ray spectra from $\bar{p}^3$He and $\bar{p}^4$He at 72 mbar are shown (measurement II). Here, the energy range could be extended down to about 1 keV, because the detector Si II was flanged directly to the target chamber.

All detectors were supplied with an optical–feedback reset to reject signals induced by charged annihilation products. A large source of background is the neutral component of electro–magnetic shower cascades induced by γ–rays of π^0 decay. The background, observed in the 10 keV region, is underestimated by at least two orders of magnitude, if attributed to Compton induced events from the γ–rays. The spatial extension of the shower leads to multiple hits of X–rays passing the detector surface (especially for the very intense low energy part). Therefore, using guard–ring detectors, a suppression of the shower induced events proportional to the ratio of the area of the inner part to the total area of the detector is obtained.

3. Results and discussion

3.1 X–ray yields

The measured X–ray yields for antiprotonic ^{3}He and ^{4}He are summarized in table 2. The yields, as shown in fig. 3, are in good agreement with a cascade–model prediction which includes molecule–ion formation [11]. The increasing yields clearly show the decreasing influence of the Stark effect with decreasing pressure. Saturation, however, is not reached even at 36 mbar. The electro–magnetic cascades of $\bar{p}^3$He and $\bar{p}^4$He are equal within the experimental errors. The slightly smaller yield of the $\bar{p}^4$He Lα transition can be attributed to the larger hadronic width of the 3d level. In comparison with the $\bar{p}^4$He yields measured by LEAR experiment PS174 in the pressure range from 125 mbar to 10 bar [13], the results of this experiment exhibit about 30 % smaller yields for the circular transitions $((n,\ell{=}n{-}1) \rightarrow (n{-}1,\ell{=}n{-}2))$.

3.2 Strong–interaction energy shift and broadening

The measured energies for those transitions not affected by strong interaction (the N and M series) agree with those calculated using the computer code PBAR [14] or the results taken from [15,16]. The accuracy of the energy determination ranges from 5 to 15 eV for the various detectors, measuring periods, and transition energies, including about 3 eV from the uncertainty of the energy calibration.

The shape of the lines, except for the L series, is well described by the gaussian–shaped response function of the detectors obtained from the in–beam calibrations.

The transition energies of the L series are shifted compared with those predicted by the electro–magnetic interaction only. In addition, the line shapes of the Lα transitions cannot be described by a pure gaussian, but are well described by Voigt profiles (folding of a gaussian and Lorentzian). This is shown in fig. 4. No significant improvement of the fit of the hadronic width has been obtained by including the fine– and hyperfine–structure splitting of the 2p–levels as given by Barmo et al. [15].

The hadronic width of the 3d level is obtained from the intensity balance of the M series and the Lα transition. The measured line intensities have to be corrected for non radiative transitions, i.e. internal and external Auger transitions or collisional de-excitation. At the low pressures used in this experiment, the rates of the non–radiative transitions are suppressed by at least 3 orders of magnitude to the radiative transitions. The contribution of parallel transitions (n, $\ell <$ n–1) $\rightarrow$ (n–1, $\ell <$ n–2), which cannot be resolved experimentally from the circular ones (n, $\ell =$ n–1) $\rightarrow$ (n–1, $\ell =$ n–2), has been determined from $\Delta n \geq 2$ transitions. The contribution to the Mα transition at 72 mbar gas pressure is (1.6 ± 0.3)% for ^{4}He and (1.1 ± 0.2)% for ^{3}He. The total intensity of the higher M–series transitions ($\Delta n \geq 5$) is estimated from the observed transitions Mγ, Mδ and Mϵ to be less than 3%. The population of the 3d level P_{3d} is then given by the total X–ray yield of the M series corrected for the parallel transitions. The hadronic width is obtained from the relation $\Gamma_{3d} = \Gamma_{3d}^{rad} \cdot (P_{3d}/Y_{3d\text{-}2p}-1)$, where the radiative widths Γ_{3d}^{rad} including the Fried–Martin correction [17] are 1.56 meV for $\bar{p}^3$He and 1.44 meV for $\bar{p}^4$He.

The hadronic shifts of the 2p levels and the widths the hadronic of 2p and 3d levels are given in table 3. It can be seen that the strong interaction parameters determined in this experiment all agree within the errors for the various detectors and target pressures. From these results weighted averages have been calculated. Theoretical predictions of hadronic shifts and widths and the results of the other experiments are also included in table 3. From the 2p level widths a yield of a few 10^{-4} is deduced for the Kα transitions at 72 mbar. The expected hadronic width of the 1s level is several keV thus making the observation of the Kα transitions with present techniques impossible.

3.3 Comparison with theoretical predictions of strong–interaction effects

Three different approaches have been used to predict level shifts and widths of antiprotonic helium (see also tab. 3):

(i) Assuming only a universal effective absorption strength, which corresponds to a mean free path of the antiproton in matter of about 1.2 nucleon diameters (black–sphere model), the gross features of the annihilation widths are already reasonably well described over a wide range of the periodic table [19]. The 3d level width is overestimated in this model, but can be decreased by introducing an effective weakly attractive real potential.

(ii) The phenomenological approach of an optical potential $U(r)= -(2\pi/\mu)(1+\mu/m)\, a_{eff}\, \rho(r)$ reduces the description of the $\bar{p}$–atom interaction to a complex effective scattering length a_{eff}. For the nuclear matter distribution $\rho(r) = \rho_p(r) + \rho_n(r)$ we used a harmonic–well density distribution, $\rho_n = (N/Z)\cdot\rho_p$, where $\rho_p(r) = [1 + \frac{Z-2}{3}(r/R)^2] \exp[-(r/R)^2]$ is the charge distribution. The root mean square radii R of the nuclei are obtained from electron scattering [20]. Solving the Klein– Gordon equation including U(r) leads to effective scattering lengths $a_{eff} = [(-0.7 \pm 2.9) + i(8.5 \pm 2.9)]$fm for ^{3}He and $[(1.5 \pm 1.1) + i(5.5 \pm 1.6)]$fm for ^{4}He. Shifts and widths obtained with these parameters are added in table 3 (further details see [8]). Here the 2p shift and width as well as the 3d width have been used to avoid the ambiguities arising from the eigenmodes of the potential [8,21–23]. These ambiguities, leading to the so called shallow potential, disappear when the number of input data sets is increased. Using both isotopes $a_{eff}=[(1.4\pm0.4)+i(5.8\pm0.4)]$ is obtained. With a large data base from antiprotonic atoms with $A \geq 6$, Batty obtained $a_{eff}=[(1.5\pm0.3)+i(2.5\pm0.3)]$fm [24,25]. With this effective scattering length the

experimental results of the experiments performed at LEAR (PS 174 [18] and PS 175 (this work)) can be reproduced within a factor of 2. Shift and widths, however, are not very sensitive to a_{eff} as can be seen from table 3.

(iii) From a (microscopic) optical potential, derived from a basic $\bar{N}N$ interaction [2], the width Γ_{2p} of $\bar{p}^4$He is described well, whereas the shift is about half of the value obtained in this experiment. The effects due to the spin–orbit and tensor part of the interaction are predicted to be negligibly small for $\bar{p}^4$He.

As a general trend, both the phenomenological optical potential [8,25] and the optical potential constructed from the 2–body interaction [2] underestimate the 2p shifts. Even a dedicated fit to $\bar{p}^4$He of the optical potential underestimates the absorption from the 2p level by a factor of 2 [8]. The imaginary parts of a_{eff} are not conclusive to the ratio of the hadronic widths of the isotopes.

The broadening of the atomic levels is related to the reduced mass $\mu_{\bar{p}A}$ and the nuclear–matter distribution

$$\rho(r) \propto (\mu_{\bar{p}A})^{2l+2}\, \mathrm{Im}\, \bar{a}_l \cdot \int d\bar{r}\, \rho(r) \exp\left(-\frac{2r}{B\bar{n}}\right)\left(1-\alpha_l \frac{r}{B\bar{n}}\right).$$

Here $\bar{a}_l$ is the effective scattering length, B the Bohr radius of the $\bar{p}$A system, and n the principal quantum number [1,26]. The large value of Γ_{3d} of $\bar{p}^3$He, almost equal to that of $\bar{p}^4$He indicates a much larger absorption from the 3d level in ^{3}He than would be expected from the scaling of the overlap of nuclear and antiprotonic wave functions. On the other hand, the ratio of the 2p widths is in agreement with the scaling of the mass of the exotic atom [26]. Taking into account the nuclear–matter distributions (see [1], appendix A.2), the ratios of the hadronic widths increase slightly, but cannot explain the large value for the 3d level (tab. 4). The same nuclear matter distributions have been used as for the fit of the phenomenological optical potential.

4. Summary

The strong–interaction 2p shifts and widths and 3d widths of the antiprotonic helium isotopes have been measured with semiconductor detectors. While the widths of $\bar{p}^4$He, calculated from a microscopic optical potential and the black–sphere model, agree with the measured widths, the agreement on the 2p shifts between theoretical calculations

and the experimental results is not satisfactory. The phenomenological optical potential ansatz fails to describe the strong–interaction effects in the antiprotonic helium isotopes. Detailed microscopical model calculations are required. Neither the hyperfine or fine structure cannot be resolved within the experimental accuracy, which is, however, the limit attainable with Si(Li) detectors. The experimental errors could be reduced by at least one order of magnitude if a crystal spectrometer is used to measure the line shapes of the Lα transitions [27].

The efforts of the LEAR staff and the help of P. Gauss from the CERN Cryogenic Group as well as the technical assistance of M. Dröge and M. Stoll are gratefully acknowledged. This work is part of the Ph.D. of one of us (M.S.), University of Karlsruhe (1987), KfK report no. 4222.

References

1) A.M. Green and S. Wycech, Nucl. Phys. A377 (1982) 441
2) O. Dumbrajs, H. Heiselberg, A.S. Jensen, A. Miranda, G.C. Oades, and J.M. Richard, Nucl. Phys. A457 (1986) 491
3) A.M. Green and J.A. Niskanen, Prog. in Part. and Nucl. Phys., vol. 18 (1987) 93
4) H. Poth, R. Abela, G. Backenstoss, P. Blüm, W. Fetscher, R. Hagelberg, M. Izycki, H. Koch, A. Nilsson, P. Pavlopoulos, L. Simons, and L. Tauscher, Phys. Lett. 76B (1978) 523
5) R.W. Wodrich, E.G. Auld, J.M. Bailey, G.A. Beer, B. Dreher, U. Gastaldi, H. Kalinowsky, E. Klempt, R. Landua, K. Merle, K. Neubecker, Chr. Saber, R.D. Wendling, and B.L. White, Nucl. Phys. A384 (1982) 386
6) S. Baird, C.J. Batty, F.M. Russell, P. Sharman, P.M. Bird, A.S. Clough, K.R. Parker, G.J. Pyle, and G.T.A. Squier, Nucl. Phys. A392 (1983) 297
7) L.M. Simons, R. Bacher, P. Blüm, D. Gotta, W. Kunold, and M. Schneider, hopefully to be published
8) M. Schneider, thesis, University of Karlsruhe 1987, KfK report no. 4222, 1987
9) R. Bacher, P. Blüm, D. Gotta, K. Heitlinger, M. Schneider, J. Missimer, L.M. Simons, and K. Elsener, Phys. Rev. A38 (1988) 4395
10) R. Bacher, P. Blüm, D. Gotta, K. Heitlinger, D. Rohmann, M. Schneider, J. Egger, L.M. Simons, and K. Elsener, Z. Phys. A334 (1989) 93
11) G. Reifenröther, E. Klempt, and R. Landua, Phys. Lett. B203 (1988) 9
12) G. Reifenröther, E. Klempt, and R. Landua, Phys. Lett. B191 (1987) 15
13) C.A. Baker, C.J. Batty, J. Moir, S. Sakamoto, J.D. Davies, J. Lowe, J.M. Nelson, G.J. Pyle, G.T.A. Squier, R.E. Welsh, R.G. Winter and E.W.A. Lingeman, Nucl. Phys. A494 (1989) 507
14) E. Borie and B. Jödicke, Comp. Phys. Vol. 2, no. 6 (1988) 61
15) S. Barmo, H. Pilkuhn, and H.G. Schlaile, Z. Phys. A301 (1981) 283
16) G. Bohnert, R. Decker, A. Hornberg, H. Pilkuhn, and H.G. Schlaile, Z. Phys. D2 (1986) 23
17) Z. Fried and A.D. Martin, Nuovo Cimento 29 (1963) 574
18) J.D. Davies, T.P. Gorringe, J. Lowe, J.M. Nelson, S.M. Playfer, G.J. Pyle, G.T.A. Squier, C.A. Baker, C.J. Batty, S.A. Clark, S. Sakamoto, R.E. Welsh, R.G. Winter, and E.W.A. Lingeman, Phys. Lett. 145B (1984) 319
19) W.B. Kaufmann and H. Pilkuhn, Phys. Lett. 166B (1986) 279
20) J.S. McCarthy, I. Sick, and R.R. Whitney, Phys. Rev. C15 (1977) 1396
21) M. Krell, Phys. Rev. Lett. 26 (1971) 584
22) Ch.–Y. Wong, A.K. Kerman, G.R. Satchler, and A.D. McKellar, Phys. Rev. C29 (1984) 574
23) C.J. Batty, Nucl. Phys. A372 (1981) 418
24) C.J. Batty, Nucl. Phys. A372 (1981) 433
25) C.J. Batty, Nucl. Phys. A508 (1990) 89c
26) E. Lambert, Helv. Phys. Acta 43 (1970) 713
27) D. Anagnostopoulos, G.L. Borchert, D. Gotta, O.W.B. Schult, L.M. Simons, K. Elsener, K. Rashid, J.J. Reidy, R.D. Deslattes, T. Mooney, P. Cowan, P. Indelicato, E.D. Bovet, D. Chatellard, J.–P. Egger, and E. Jeannet, CERN/PSCC/90–9/P124

Table 1: **Set–up parameters of the X–ray detectors for the various measuring periods.**

set-up/detector	Si I	Si II	Si III	Ge I	Ge II
detector type	Si(Li) planar	Si(Li) guard-ring	Si(Li)	intrinsig Ge planar	intrinsic Ge guard-ring
beam momentum /MeV/c	309	202	202	202	202
measuring period	I	II	III	II	III
target pressure/mbar	375/600	72	36	72	72
^{3}He: incoming $\bar{p}/10^9$	–	1.544	–	1.544	–
^{4}He: "	2.661	2.537	0.078	2.537	0.078
inner/outer area/mm²	30	30/200	300	200/500	200/900
Be-window thickness/μm	8	12	50	130	500
resolution at 5.9 keV/eV	160	200	460	250	365
$\Delta\Omega/4\pi$	$9\cdot10^{-5}$	$1.2\cdot10^{-5}$	$1.1\cdot10^{-3}$	$7.8\cdot10^{-5}$	$1.4\cdot10^{-4}$

Table 2: **Measured absolute yields of antiprotonic X–ray transitions from $\bar{p}^3$He and $\bar{p}^4$He.**

	Y/%				
	$\bar{p}^3He$	$\bar{p}^4He$			
	72 mbar	600 mbar	375 mbar	72 mbar	36 mbar
$L\alpha$	26 ± 4	13 ± 3	10 ± 3	21 ± 3	23 ± 2
$L\beta$	1.9 ± 0.5	1.5 ± 0.4	2.0 ± 1.5	2.2 ± 0.5	0.8 ± 0.2
L_{tot}	33 ± 8	–	–	33 ± 7	25 ± 2
$L\beta/L\alpha$	7.3 ± 2.2	12 ± 4	20 ± 16	11 ± 3	3.5 ± 0.9
$M\alpha$	45 ± 6	30 ± 7	24 ± 6	43 ± 4	48 ± 9
$M\beta$	8.2 ± 1.5	4.5 ± 1.2	2.0 ± 1.2	5.5 ± 1.3	4.0 ± 0.4
$M\gamma$	2.3 ± 0.7	1.5 ± 0.9	1.1 ± 0.9	2.2 ± 0.4	1.4 ± 0.2
M_{tot}	64 ± 11	35 ± 9	26 ± 8	57 ± 6	57 ± 3
$M\beta/M\alpha$	18 ± 4	15 ± 5	8.3 ± 5.3	13 ± 3	8.3 ± 1.8
$N\alpha$	32 ± 9	–	–	37 ± 3	–
$N\beta$	5.7 ± 4.3	–	–	7.6 ± 2.9	–
N_{tot}	42 ± 12	–	–	52 ± 16	–
$N\beta/N\alpha$	18 ± 15	–	–	21 ± 8	–

Table 3: Measured strong interaction 2p shifts ϵ_{2p} and 2p and 3d widths Γ_{2p} and Γ_{3d} of $\bar{p}^3$He and $\bar{p}^4$He (* the analysis in ref. [5] was performed without Fried–Martin factor). The electro–magnetic transition energies of the Lα transitions are 10.440 keV for $\bar{p}^3$He and 11.129 keV for $\bar{p}^4$He [14,15]. In the analysis of PS174 [18] the electro–magnetic energy for the $\bar{p}^4$He Lα transition was taken to be 11.131 keV. The theoretical predictions are from the black–sphere model [19], optical–potential fits [25], and a microscopic optical–potential calculation [2]. An optical potential fit to the helium isotopes separately has been performed in [8].

	detector, theoretical model	p mbar	ϵ_{2p} eV	Γ_{2p} eV	Γ_{3d} meV	ref.
$\bar{p}^3He$	Si II	72	-11 ± 11	54 ± 26	2.16 ± 0.25	this exp.
	Ge I	72	-18 ± 4	22 ± 9	2.12 ± 0.25	
	weighted average		-17 ± 4	25 ± 9	2.14 ± 0.18	
	opt. potential fit		-16	21	2.15	[8]
	opt. potential fit		-6 ± 1	24 ± 2	1.30 ± 0.15	[25]
$\bar{p}^4He$	Si I	375/600	-18 ± 6	40 ± 18	2.42 ± 0.19	this exp.
	Si II	72	-19 ± 9	45 ± 16	2.32 ± 0.22	
	Si III	36	-21 ± 4	49 ± 6	2.21 ± 0.16	
	Ge I	72	-15 ± 4	38 ± 10	2.53 ± 0.22	
	Ge II	36	-23 ± 7	33 ± 18	–	
	weighted average		-18 ± 2	45 ± 5	2.36 ± 0.10	
		LHe	-50 ± 18	90 ± 70	–	[4]
		1100/4000	-14 ± 6	–	$2.8 \pm 1.0^*$	[5]
		LHe	-12 ± 14	0^{+30}_{-0}	–	[6]
		10^4	7.4 ± 5.3	35 ± 15	2.4 ± 0.5	[18]
		$125 - 10^4$	–	–	2.07 ± 0.11	[13]
	opt. potential fit		-15	25	2.37	[8]
	opt. potential fit		-8 ± 1	25 ± 2	1.67 ± 0.16	[25]
	mean free path		–	42	3.2	[19]
	microscopic opt. p.		-6	38	–	[2]

Table 4: Ratios of the hadronic 2p and 3d widths. The ratios are calculated from the scaling of the wave functions with and without taking into account the different nuclear–matter distributions.

	this experiment	scaling of wave functions	scaling and nucl.–matter distr.
$\Gamma_{2p}(^3He)/\Gamma_{2p}(^4He)$	0.56 ± 0.21	0.61	0.69
$\Gamma_{3d}(^3He)/\Gamma_{3d}(^4He)$	0.92 ± 0.09	0.55	0.63

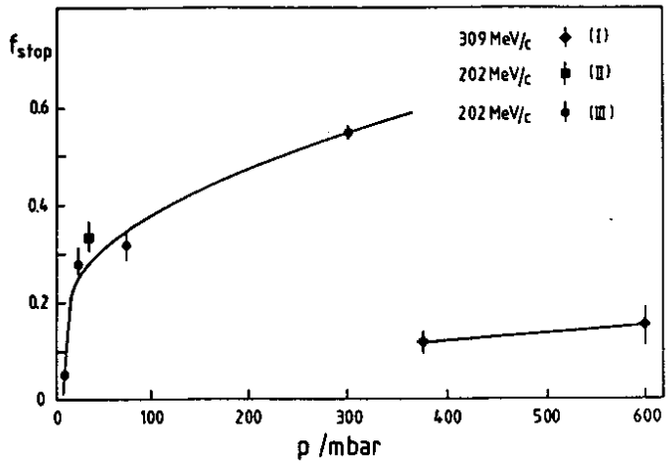

Fig. 1: Stop efficiency of the cyclotron trap in the measuring periods I,II and III.

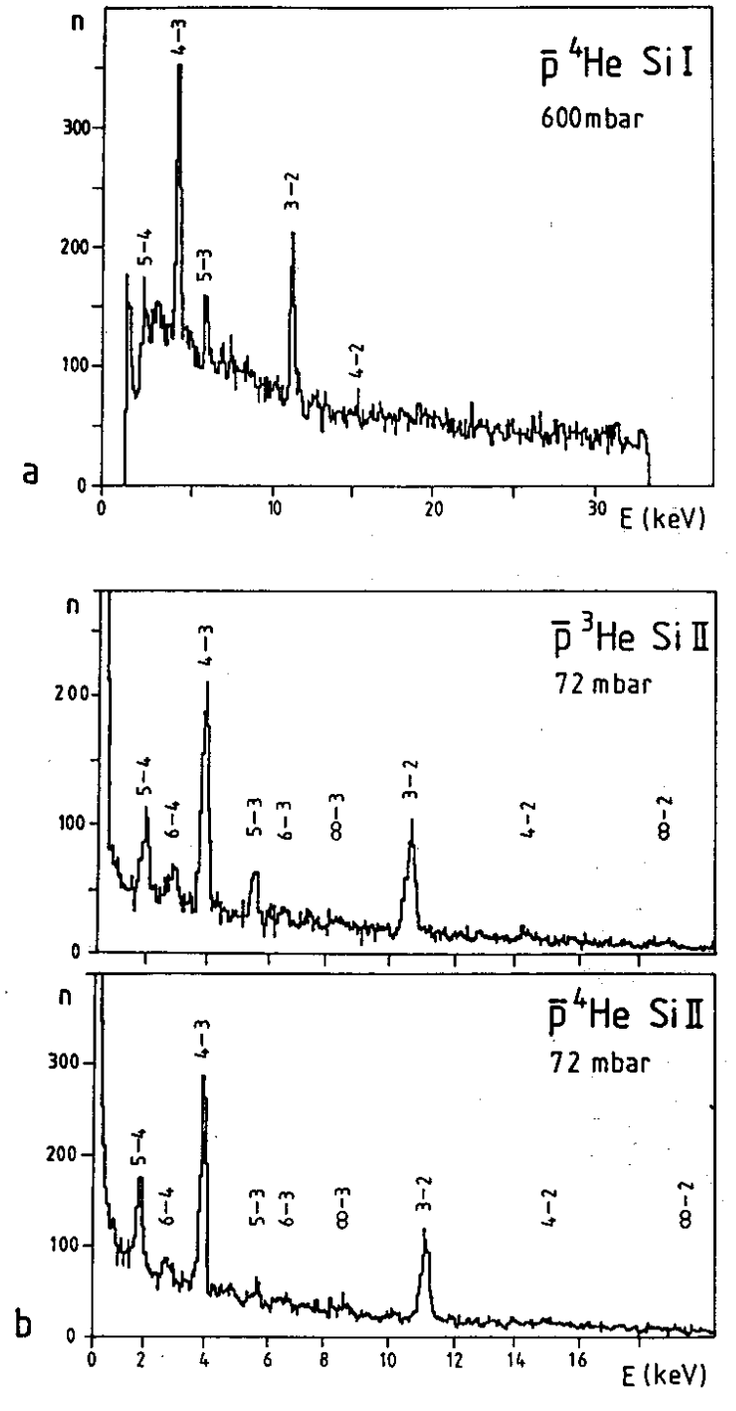

Fig. 2: (a) X-ray spectrum of $\bar{p}^4$He at 600 mbar measured with detector Si I.
(b) X-ray spectra of $\bar{p}^3$He at 72 mbar measured with Si II.

Imprimé au CERN. Prix : 0.40 Fr.

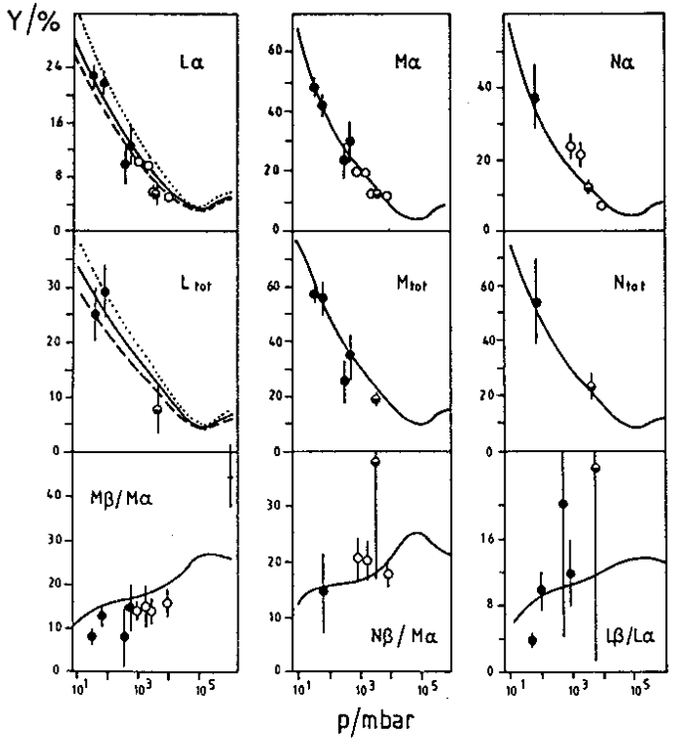

Fig. 3: Measured X-ray yields of $\bar{p}^4$He compared to the cascade calculations of [11] (• : this experiment, + : [4], ⊛ : [5], o : [13], ... : Γ_{2p} = 1.9 meV, — : Γ_{2p} = 2.4 meV, –– : Γ_{2p} = 2.9 meV).

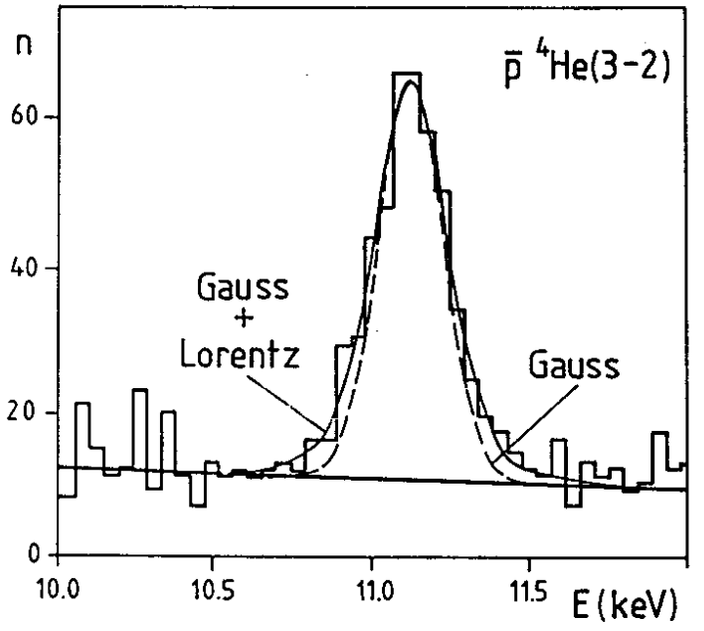

Fig. 4: Fit to the line profile of the $\bar{p}^4$He Lα transition (Si II). The deviation from the pure gaussian response function of the detector shows the influence of the strong-interaction braodening.